Substructural Properties and Anisotropic Peak Broadening in $Zn_{1-x}Mn_xTe$ Films Determined by a Combined Methodology Based on SEM, HRTEM, XRD, and HRXRD

C. Martinez-Tomas, O. Klymov, S. Agouram, D. Kurbatov, A. Opanasyuk & V. Muñoz-Sanjosé

Metallurgical and Materials Transactions A

ISSN 1073-5623

Metall and Mat Trans A
DOI 10.1007/s11661-016-3762-6

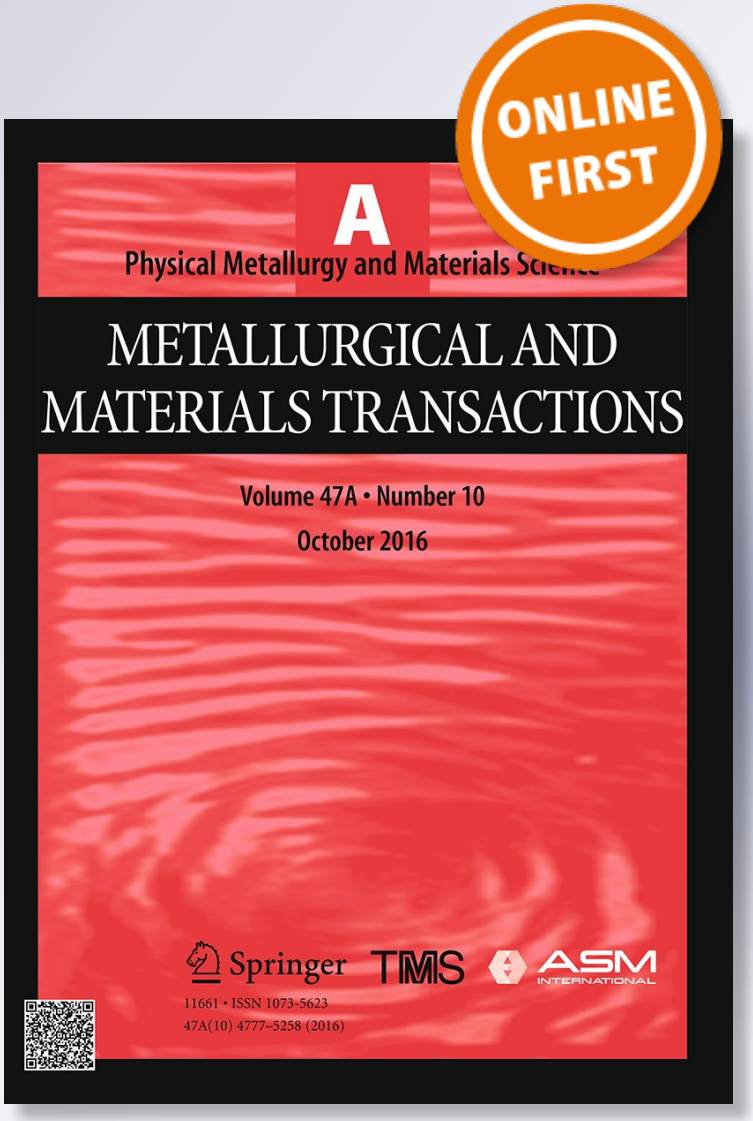

Springer

Substructural Properties and Anisotropic Peak Broadening in $Zn_{1-x}Mn_xTe$ Films Determined by a Combined Methodology Based on SEM, HRTEM, XRD, and HRXRD

C. MARTINEZ-TOMAS, O. KLYMOV, S. AGOURAM, D. KURBATOV, A. OPANASYUK, and V. MUÑOZ-SANJOSÉ

Lattice deformation and extended defects such as grain boundaries and dislocations affect the crystalline quality of films and can dramatically change material's properties. In particular, magnetic and optoelectronic properties depend strongly on these structural and substructural characteristics. In this paper, a combined methodology based on SEM, HRTEM, XRD, and HRXRD measurements is used to determine and assess the structural and substructural characteristics of films. This combined methodology has been applied to $Zn_{1-x}Mn_xTe$ films grown on glass substrates by close-spaced vacuum sublimation. Nevertheless the methodology can be applied to a wide variety of materials and could become a useful characterization method which would be particularly valuable in semiconductor growth field. The knowledge of the structural and substructural characteristics can allow not only the optimization of growth parameters, but also the selection of specific samples having the desired characteristics (crystallite size, minimum dislocation content, *etc.*) for high-quality technological devices.

DOI: 10.1007/s11661-016-3762-6

I. INTRODUCTION

IN order to obtain highly efficient devices, it is essential to ensure a high-crystalline quality of micro- or nanocrystals. However, lattice deformations and extended defects such as grain boundaries and dislocations (known as substructural characteristics) affect the crystalline quality and can dramatically change material's properties and affect device's performance.[1] It is therefore very important to detect and analyze the structural and substructural characteristics in semiconductor films; consequently, an efficient, fast, and nondestructive methodology for this type of characterization is fundamental.

There are several effective characterization tools. However, as each one of them provides different information, a combined methodology is needed to reach a complete characterization. Scanning electron microscopy (SEM) and transmission electronic microscopy (TEM) allow the determination of particle size of individual particles in the nano- and submicron range. As well, TEM can provide images of lattice defects, but it is limited to isolated grains or particles. On the contrary, X-ray diffraction methods (XRD) provide statistical values. Mean values for crystallite size and lattice distortion can be obtained by the conventional Williamson–Hall (CWH) analysis of XRD peak broadening. Nevertheless, the CWH analysis is limited to isotropic diffraction.[2–4] When the material presents the anisotropic diffraction, this analysis can not be made and it has to be updated by taking into account the differentiated effect (contrast) of dislocations on peak broadening.[5,6]

It is not difficult to find in the literature how the use of single characterization techniques can produce misleading interpretations and confusing conclusions. The aim of this work is to apply a combined sequenced methodology, based on the use in conjunction of several characterization techniques, which will allow the complete determination and assessment of structural and substructural characteristics of films.

This methodology has been applied to the study of $Zn_{1-x}Mn_xTe$ films. $Zn_{1-x}Mn_xTe$ is a ternary semiconductor (from now, ZnMnTe) that belongs to the group of diluted magnetic semiconducting alloys that have attracted much attention due to its semimagnetic character.[7] The partial substitution of the Zn cation by Mn results in a $sp-d$ hybridization, giving rise to interesting magneto-optical and magneto-transport properties.[8] Among other growth methods, films of this ternary compound are mostly obtained by pulsed laser deposition,[9] flash evaporation,[10] high-frequency magnetron scattering,[11] or metalorganic vapor phase epitaxy.[12] In

C. MARTINEZ-TOMAS, Full Professor, S. AGOURAM, Research Associate, and V. MUÑOZ-SANJOSÉ, Full Professor, are with the Departamento de Física Aplicada y Electromagnetismo, Universidad de Valencia, Burjassot 46100, Spain. Contact e-mail: Carmen.Martinez-tomas@uv.es O. KLYMOV, Ph.D Student, D. KURBATOV, Chief of Science and Research Department, and A. OPANASYUK, Head of the Department of Electronics and Computer Technology, are with the Department of Electronics and Computer Technology, Sumy State University, Sumy 40007, Ukraine.

Manuscript submitted September 30, 2015.

Published online: 19 September 2016

this work, we have used the close-spaced vacuum sublimation (CSVS) technique for the growth of ZnMnTe films on glass substrates. This method has been selected due to its simplicity, cheapness, and capacity to grow films in conditions close to thermodynamical equilibrium.[13] In the current literature, we can find the study of some structural features of ZnMnTe films[9–12] but substructural characteristics have been poorly studied. In fact, there is still some controversial about, as some authors held the idea that there is little or no dislocation in submicron materials due to the invalid assumption associated with an infinite crystal, but others claim that the substructure of grains includes dislocation.[14] In addition, the effect of Mn atoms on the structural and substructural properties of this ternary is a matter of particular interest.

The aim of this work is making a complete structural and substructural characterization of ZnMnTe films using a combined methodology that allows a knowledge of this type of characteristics. It is worth to note that this methodology can be applied to a wide variety of materials and could become a useful characterization method which would be particularly valuable in the semiconductor growth field.

II. EXPERIMENTAL

Thin ZnMnTe films were deposited, as before said, by the CSVS technique on cleaned glass substrates under residual gas pressure no more than 5×10^{-3} Pa. The detailed description of the growth setup can be found elsewhere.[15,16] ZnTe with a nominal 5 pct Mn content was evaporated at an evaporator temperature $T_e = 1073$ K (800 °C). Different substrate temperatures were studied in the interval $T_s = 623$ K to 923 K (350 °C to 650 °C); the time of evaporation was 10 minutes in all the cases.

Morphology of the samples was studied through scanning electron micrographs using a Hitachi S-4800 field-emission SEM with an acceleration voltage of 20 kV. High-resolution transmission electron micrographs, energy-dispersive X-ray analysis (EDAX), and selected area electron diffraction were recorded using a Tecnai G2 F20 field-emission gun TEM under an acceleration voltage of 200 kV. For TEM and EDAX measurements, ZnMnTe particles were removed using a clean surgical blade and deposited onto a TEM support carbon film on a copper grid (C-grid).

XRD and HRXRD measurements were performed with a Bruker D8 Advanced A25 diffractometer equipped with a Lynx eye fast detector (3 deg of aperture) and a PANalytical X'Pert MRD diffractometer, respectively. The instrumental broadening for correction of the full width at half maximum (FWHM) was determined from diffraction lines of a LaB6 reference sample. Decomposition of peaks was made from the fitting of the whole pattern and the subtraction of the instrumental broadening. Film orientation was characterized by $2\theta - \theta$ scans, texture coefficients, modified Williamson–Hall plots, and pole figure analysis.

III. RESULTS

A. *Morphological Study*

SEM measurements can produce vivid images of a sample surface. Thus, usually the first investigation of films begins with the analysis of its morphology in order to study the structure evolution as a function of growth parameters, in our case the substrate temperature. Figure 1 depicts the SEM micrograph of ZnMnTe films grown over glass at various substrate temperatures. Grains in the range from 600 to 800 nm with a density from of 2×10^{12} to 1×10^{12} NPs/m^2, respectively, can be observed in the selected substrate temperatures values. They seem to be randomly distributed, without any organization over the substrate. The cross-sectional study of samples shows that grains are columnar thus the aforementioned size refers to the width of the columnar grains.

Crystalline grains in the submicron range may be constituted by several crystallites, defined also as single-phase regions separated by grain boundaries.[17] Consequently the obtained values by SEM can only be considered as values related to the overall size of a grain. If they have a single or polycrystalline structure, it can be only assessed by XRD and/or HRTEM measurements, as we will study in Section III–D.

B. *Lattice Constant and Mn Content*

The crystallinity of a doped material is generally decreased as a consequence of the dopant penetration. XRD measurements can assess the degree of distortion in the parent lattice which additionally can affect the substructural characteristics of material. Figure 2 shows conventional $2\theta - \theta$ patterns from ZnMnTe films grown at different substrate temperatures. Diffraction peaks indicate that all samples have cubic structure with an apparent (111) preferred orientation as found also by other authors.[18] No diffraction peaks of impurity phases were found in the samples, suggesting that Mn^{2+} ions substitute into the Zn^{2+} sites. The positions of the diffraction peaks correspond to the crystallographic card of ZnTe (JCPDS-ICCD No 00-015-0746).

The lattice parameter for each sample was obtained by plotting the diffraction order $(h^2 + k^2 + l^2)$ *vs* $2 \times \sin\theta \times 1/\lambda$ where θ is the Bragg angle and λ the wavelength of the X-ray beam. Calculated values of the lattice parameter as a function of the substrate temperature are shown in Table I and Figure 3(a) (as a general rule, uncertainties have been determined by using the error propagation theory of experimental errors). It is observed that at a substrate temperature of 623 K (350 °C), the lattice constant is higher than the value given by the crystallographic card, being this enlargement indicative of the Mn incorporation. However, this incorporation decreases as the substrate temperature increases, as it will be discussed later.

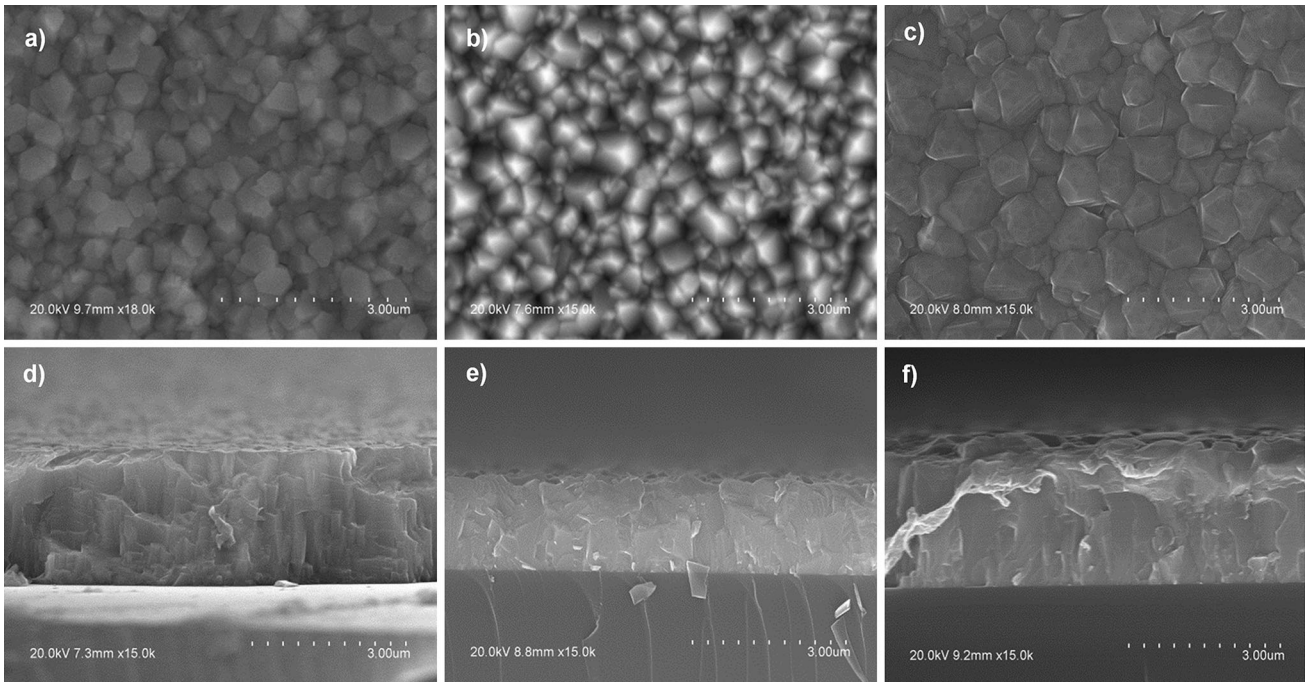

Fig. 1—Top (upper) and cross-sectional (lower) SEM images obtained from the ZnMnTe films deposited over glass at various substrate temperatures: (*a*, *d*) T_s = 623 K (350 °C); (*b*, *e*) T_s = 773 K (500 °C); (*c*, *f*), T_s = 923 K (650 °C).

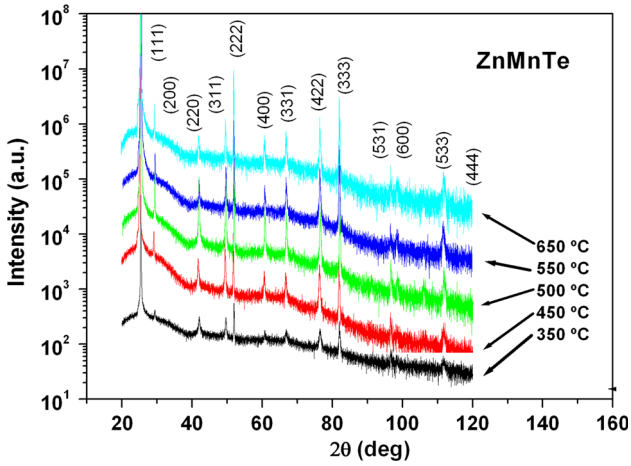

Fig. 2—X-ray diffraction patterns from ZnMnTe films deposited over glass at various substrate temperatures: 623 K, 723 K, 773 K, 823 K, and 923 K (350 °C, 450 °C, 500 °C, 550 °C, and 650 °C).

The effect of Mn atoms on the ZnTe lattice can be analyzed from a comparison among ionic radii. The crystal ionic radius of Zn^{2+} ions is 88 pm but that of Mn depends on the coordination number and the spin states of the ions.[19] In Mn^{2+} ions, the crystal ionic radius for the low spin state is 81 pm and for the high spin sate is 97 pm. The large value of the lattice constant with the presence of manganese suggests that the Zn^{2+} ions are partially substituted by the bigger Mn^{2+} ones, that is, those with a high spin state. The increasing of the lattice constant with the Mn content has been found also by other authors during the growth of ZnMnTe ingots.[20] When a shortening has been observed,[21] it has been explained as a residual thermal strain that was not ruled out.

A calculated value for the Mn incorporation can be obtained from the Vegard's law. This law is an approximate empirical rule which holds that a linear relation exists, at constant temperature, between the crystal lattice constant of an alloy and the concentrations of the constituent elements. For the ZnMnTe case,

$$a(Zn_{1-x}Mn_xTe) = x \cdot a(MnTe) + (1-x)\, a(ZnTe), \quad [1]$$

where we will take the lattice constant of the parent binary compounds, *a*(MnTe) and *a*(ZnTe), as those corresponding to the zinc-blende phase (0.6105 and 0.6337 nm), respectively.[22,23] The values *x* of the Vegard's law are reflected in Table I and Figure 3(b).

Experimental values of Mn content can be obtained from energy-dispersive X-ray spectroscopy (EDS) coupled with HRSEM. These measurements confirm the partial incorporation of Mn in the ZnTe lattice, as can be seen in Table I. Although the trend is the same, the interval of the EDS values (0.7 to 2.1 pct) is lower than that obtained by the Vegard's law (0 to 3.7 pct). These quantities are lower than the nominal value (5 pct) thus indicating the reluctance of the ZnTe lattice to incorporate Mn atoms.

C. *Out-Plane and In-Plane Orientation of Films*

The high intensity of the (111) peaks in XRD patterns suggests an out-plane preferred orientation. However, this can only be confirmed from texture analysis.[24] In this type of analysis, texture coefficients (proportional to

Table I. Lattice Constant and Mn Content Determined by XRD and EDS in ZnMnTe Films Deposited Over Glass at Various Substrate Temperatures

Substrate Temperature K (°C)	623 K (350 °C)	723 K (450 °C)	773 K (500 °C)	823 K (550 °C)	923 K (650 °C)
Lattice constant by XRD (nm) (±0.0004 nm)	0.6111	0.6107	0.6102	0.6102	0.6102
Mn content by Vegard's law (pct) (±0.1)	3.7	1.9	0	0	0
Mn content by EDS (pct) (±0.1)	2.1	2.0	0.6	0.6	0.7

the number of crystallites in a given orientation) and the degree of preferred orientation, σ (a numerical value that indicates how much a crystal is well oriented) are calculated.

Both parameters depend on the number of analyzed peaks, N. In present study, $N = 6$ since only 6 major directions are involved (111, 200, 220, 311, 331, and 422). Then for a perfectly oriented sample $\sigma = \sqrt{5} = 2.236$. Table II shows texture coefficients and preferred orientation of films, allowing an accurate comparison among samples. It can be observed in Figure 4 that at the lower temperature here considered [623 K (350 °C)], the dominant crystallographic planes of crystallites are the (111), with a σ value almost equal to that of a perfect oriented sample. As the substrate temperature increases, the number of crystallites with other orientation increases [concretely those having a (200) orientation] and σ decreases. Finally at the highest temperature [923 K (650 °C)], the value of σ is again almost equal to that of a perfect oriented sample. ZnTe has usually the (111) preferred orientation, mainly when it is doped with metals.[25]

Once the preferred orientation of films is known, the quantity of particles that have the same preferred orientation within a certain angle can be determined. Thus pole figure analyses from HRXRD measurements were performed to determine both the relative quantity of (111)-oriented crystallites and the in-plane orientation of films.

For obtaining pole figures, the rotation angle (ϕ) of the diffractometer was changed from 0 to 360 deg and the inclination angle (ψ) was changed from 0 to 90 deg, while the diffraction angle 2θ was held fixed for the reflection of interest. The experimental pole figures of the {111} reflection for all samples are shown in Figure 5. All of them exhibit a broad peak with its maximum at an inclination angle $\psi = 0$ deg and a broad ring at an inclination angle at $\psi \approx 70$ deg. As a reference, the theoretical position of poles for a perfectly oriented sample is also shown, where three poles can be observed 70 deg apart from the central one. The measured broad ring corresponds to these lateral poles, indicating a random azimuthal orientation. This is known as uniaxial orientation or fiber texture, being in this case the [111] direction the fiber axis.[26] In other words, the films posses an out-plane preferred orientation but no in-plane preferred orientation.

The area under the peak (111) is related to the amount of material that diffracts in this direction; consequently, we can use this area to evaluate the quantity of particles that are oriented within a certain inclination angle. Figure 6 supplies for all samples the calculated mean diffraction intensity in the azimuthal angle as a function of the inclination angle ψ from 0 to 90 deg. The central peak is broad, with a half-width at half maximum of about 10 deg. From the integration of this peak intensity, we can determine the percentage of (111)-oriented crystallites as the ratio of the area named A (reaching an inclination angle of 10 deg) in respect to the sum of the two areas named A and B. Results are shown in Table III for (111)-oriented crystallites within two inclination angles.

The calculated values indicate that the percentage of particles with a (111) orientation within ±10 deg is high (in the range of 83 to 92 pct) for all the substrate temperatures. The variation in the percentages is small, decreasing with the substrate temperature but finally increasing at the highest temperature of 923 K (650 °C). That is, the most of the grains (~90 pct) present a (111) preferred orientation within an inclination angle of ±10 deg in all the range of growth temperature.

Once the crystal lattice, Mn content and preferred orientation have been ascertained, substructural characteristics of films will be analyzed. This will allow the determination of the mono or polycrystalline character of grains that constitute the film.

D. *Crystallite Size and Density of Dislocations*

Substructural characteristics can be obtained, in principle, by HRTEM that allows the visualization of atomic planes within a particular grain. However, this method only could provide a mean crystallite size if at least 500 to 1000 particles are accounted for. In polycrystalline materials, as is our case, information about the average shape, crystallite size, and lattice strain can be determined by X-ray line profile analysis.[5] The kinematic theory of X-ray scattering shows that crystallite size and lattice distortion are diffraction order independent or dependent, respectively, enabling the separation of the two effects. Williamson and Hall suggested that the broadening ΔK of line profiles due to this two broadening effects can be written as

$$\Delta K = \frac{0.9}{D} + e2K, \qquad [2]$$

where $K = 2 \sin \theta/\lambda$, $\Delta K = \Delta(2\theta)\cos\theta/\lambda$, $\Delta(2\theta)$ is the full width at half maximum (FWHM) of the diffraction lines in the $2\theta - \theta$ scans, θ the Bragg angle, λ the wavelength of radiation, D the average crystallite size, and $e = \langle \varepsilon^2 \rangle^{1/2}$ the square root of the quadratic lattice microstrain (or microdeformation). This equation is known as the *classical Williamson–Hall plot* (WH) and is a linear function of K.

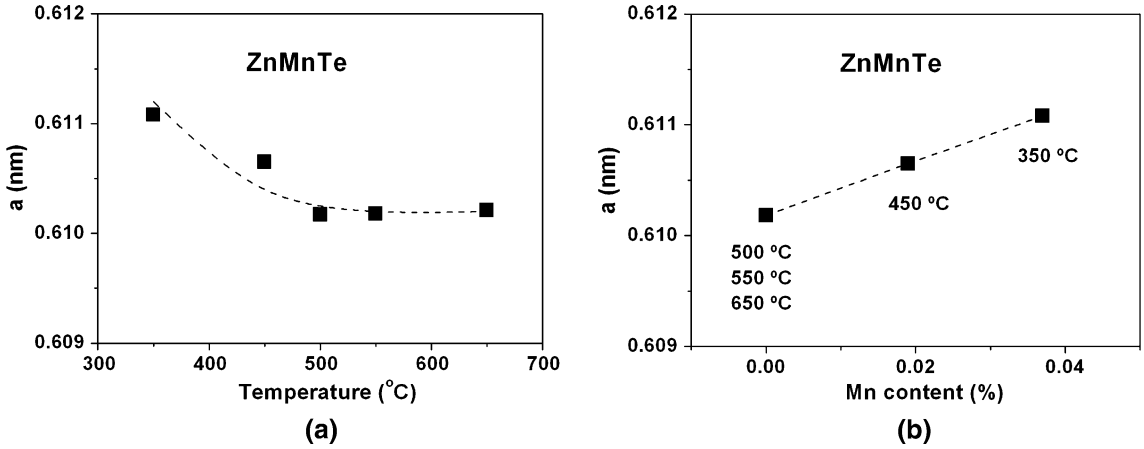

Fig. 3—Lattice constant of ZnMnTe films deposited over glass: (*a*) as a function of substrate temperature [from 623 K to 923 K (350 °C to 650 °C)]; (*b*) as a function of the Mn content, obtained from the Vegard's law.

Table II. Texture Coefficients and Preferred Orientation of a Hypothetical Perfectly Oriented Sample and of Grown Films (Uncertainties ~0.1 Percent)

	(111)	(200)	(220)	(311)	(331)	(422)	σ
Perfectly oriented							2.24
623 K (350 °C)	0.567	0.119	0.020	0.048	0.042	0.104	2.09
723 K (450 °C)	0.518	0.409	0.029	0.103	0.076	0.198	1.88
773 K (500 °C)	0.520	0.379	0.045	0.123	0.088	0.165	1.88
823 K (550 °C)	0.572	0.109	0.005	0.027	0.040	0.101	2.11
923 K (650 °C)	0.568	0.149	0.005	0.027	0.039	0.104	2.09

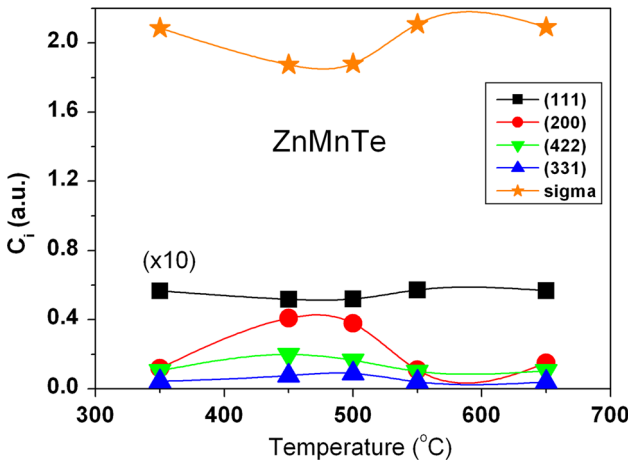

Fig. 4—Texture coefficients for some major directions obtained from ZnMnTe films deposited over glass at various substrate temperatures [from 623 K to 923 K (350 °C to 650 °C)].

This approach is useful in isotropic cases which can be interpreted with simple spherical crystallite shapes and isotropic microstrains. However, anisotropic situations require further efforts. When strain broadening is caused by dislocations, line broadening is generally anisotropic[27] and it depends on the *hkl* reflection, that is, it depends on the orientation and the length of the diffraction vector. In this case, line broadening can be described in terms of a logarithmic series expansion of the Fourier coefficients of a line profile and the average contrast factor of dislocations $\bar{C}_{hkl}$.[28] As a consequence, the proper scaling factor of breadths of peak profile is $(K\overline{C}_{hkl}^{1/2})$, instead of merely K. This is known as the *modified Williamson–Hall plot* (MWH).[29–31]

If crystallites are nonspherical, then an additional anisotropy has to be considered.[32] In such a case, crystallites can be supposed to be ellipsoidal, with their two axes dependent on the order of diffraction. Then, the crystallite size must be described by multidimensional lengths. With these considerations, the modified Williamson–Hall method can be adapted, and the line broadening can be written as

$$\Delta K = \frac{0.9}{\bar{D}_{hkl}} + \alpha K^2 \bar{C}_{hkl}, \qquad [3]$$

where $\bar{C}_{hkl}$ is the average contrast factor of dislocations for the Bragg reflection (*hkl*), $\bar{D}_{hkl}$ the average crystallite size for the Bragg reflection (*hkl*) and α is a constant depending on the Burger's vector and the density of dislocations.

The mean contrast factor $\bar{C}_{hkl}$ has been calculated taking into account that for a cubic crystal it is related to the mean contrast factor $\bar{C}_{h00}$ of the Bragg reflection (*h*00) as given by the equation

$$\bar{C}_{hkl} = \bar{C}_{h00}(1 - qH^2), \qquad [4]$$

where $H^2 = (h^2k^2 + h^2l^2 + k^2l^2)/(h^2 + k^2 + l^2)^2$ and q is a parameter which depends on the elastic constants

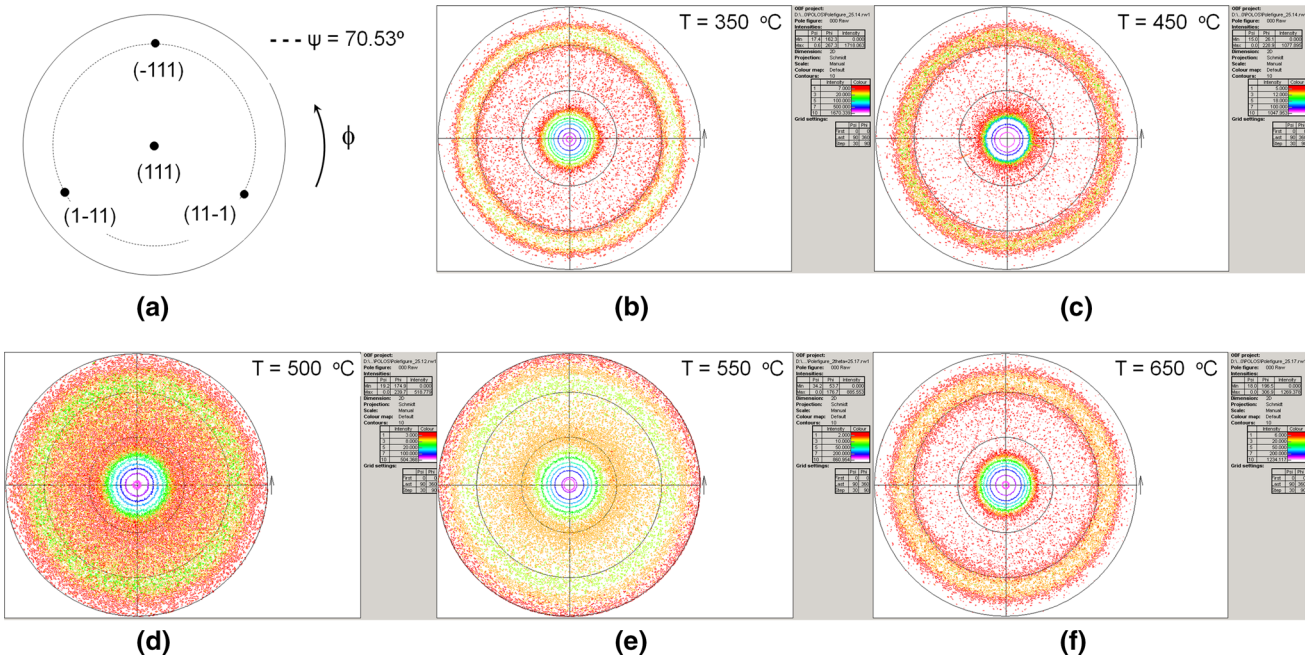

Fig. 5—Poles for the (111) reflection: (*a*) theoretical position for a perfect oriented sample in the cubic system. Experimental values for ZnMnTe films deposited over glass at various substrate temperatures: (*b*) 623 K (350 °C), (*c*) 723 K (450 °C), (*d*) 773 K (500 °C), (*e*) 823 K (550 °C), and (*f*) 923 K (650 °C).

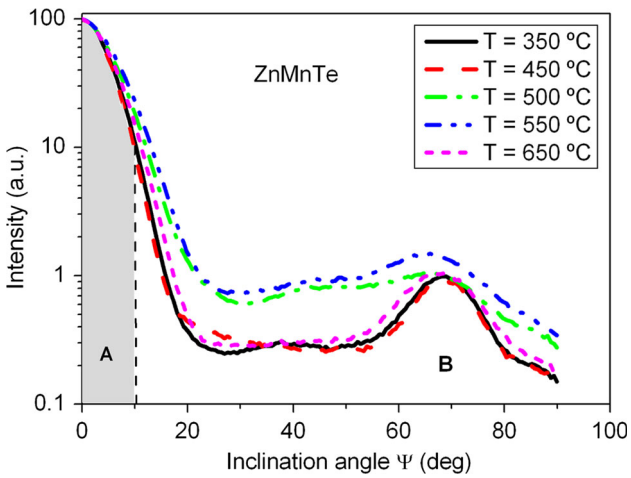

Fig. 6—Average intensity over the rotation angle of the symmetrical (111) reflection as a function of the inclination angle from ZnMnTe films deposited over glass at various substrate temperatures: *T*: 623 K (350 °C), 723 K (450 °C), 773 K (500 °C), 823 K (550 °C), and 923 K (650 °C). The area marked as A is proportional to the crystallites having a (111) orientation within ±10 deg.

and type of dislocations. The value of $\bar{C}_{h00}$ has been determined from the elastic constants of ZnTe[33] and the data given in,[34,35] resulting in $\bar{C}_{h00} = 0.24$, value which results to be the same for the two types of dislocation. On the contrary, the value of q additionally depends on the proportion between screw and edge dislocations.

The classical Williamson–Hall plot [Eq. 2] of data from ZnMnTe films grown at 923 K (650 °C) is shown in Figure 7(a) and reveals a strong anisotropy. When ΔK is plotted as a function of $K^2\bar{C}_{hkl}$, in order to determine the value of α and $\bar{D}_{hkl}$ (Figure 7(b)), it can be seen that points are grouped along three straight lines with more or less the same slope, but with different intersections at $K = 0$. This indicates different crystallite sizes, depending on the order of diffraction. The longer crystallite size is that given by planes [*hhh*], followed by the corresponding to planes (*h*00), (311), and (331) and being the shorter one that defined by planes (220) and (422). Taking into account the preferred orientation and the angles between crystallographic planes, this behavior is consistent with a prismatic crystallite having the (111) orientation as the column axis. Thus, the first set of planes will define the longitudinal size of crystallite (D_{long}) and the last set of planes the transversal size (D_{transv}). The second set of planes corresponds to planes inclined in respect to the column axis (see Figure 7(c)). The obtained crystallite sizes follow the relation $D_{\text{long}} > D_{\text{inclined}} > D_{\text{transv}}$. If films are formed by such a type of crystallites, intense {*hhh*} peaks in the XRD pattern would indicate that a majority of crystallites are in vertical position, while the other low-intensity peaks would be produced by few inclined or lying crystallites, as it is the case.

The value of *q* has been obtained by inserting Eqs. [4] into [3]

$$\frac{\Delta K - 0.9/D_{hkl}}{K^2} = \alpha\bar{C}_{h00}(1 - qH^2) \qquad [5]$$

and by solving this equation in H^2 by the least-squares method (Figure 7(d)). The best linear regression provides $q \cong 2$ that indicates a clear prevalence of screw dislocations in the ZnMnTe films.[33]

Table III. Percentage of (111)-Oriented Crystallites Within a Defined Inclination Angle for ZnMnTe Films Deposited Over Glass at Various Substrate Temperatures (Uncertainties ~0.1 Percent)

Substrate Temperature K (°C)	623 K (350 °C) (pct)	723 K (450 °C) (pct)	773 K (500 °C) (pct)	823 K (550 °C) (pct)	923 K (650 °C) (pct)
Oriented within ± 10 deg	91.7	92.2	85.3	82.9	90.0
Oriented within ± 20 deg	95.5	95.4	92.8	91.9	95.3

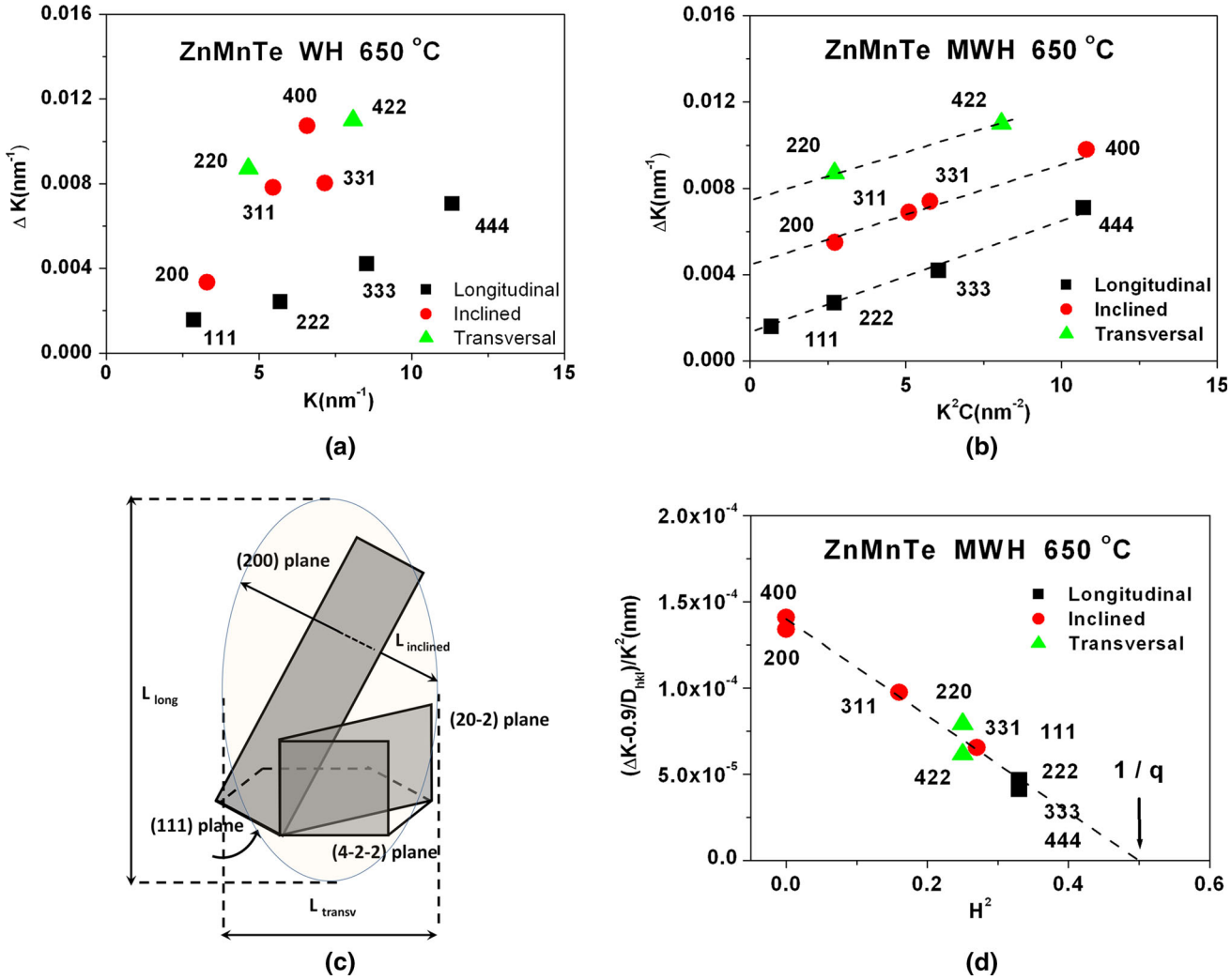

Fig. 7—From data of ZnMnTe film grown at 650 °C: (*a*) Williamson–Hall plot; (*b*) Modified Williamson–Hall plot; (*c*) some crystallographic planes in a prismatic crystallite; (*d*) plot of Eq. [3] as a function of H^2.

The mean longitudinal and transversal crystallite sizes have been calculated from XRD patterns of ZnMnTe films grown at different temperatures and are shown in Figure 8(a). The mean longitudinal size of crystallites at low temperature [623 K (350 °C)] is about 170 nm, increasing considerably with the substrate temperature. The mean transversal size also increases, but less. The aspect ratio D_{long}/D_{transv} goes from 3.5 to 5 as the temperature increases. Comparing the transversal size with values obtained by SEM, we conclude that columnar grains are polycrystalline.

If the order dependent broadening of the line profile is attributed to dislocations, according to the MWH method the slope α can be expressed[35,36] by

$$\alpha = \frac{\pi b^2 \rho^{1/2}}{2B}, \qquad [6]$$

where ρ is the dislocation density, b is the modulus of the Burger's vector of dislocation (for f.c.c. crystals $b = a/\sqrt{2}$, where a is the lattice constant) and B is a constant that can be taken as 10 for a wide range of

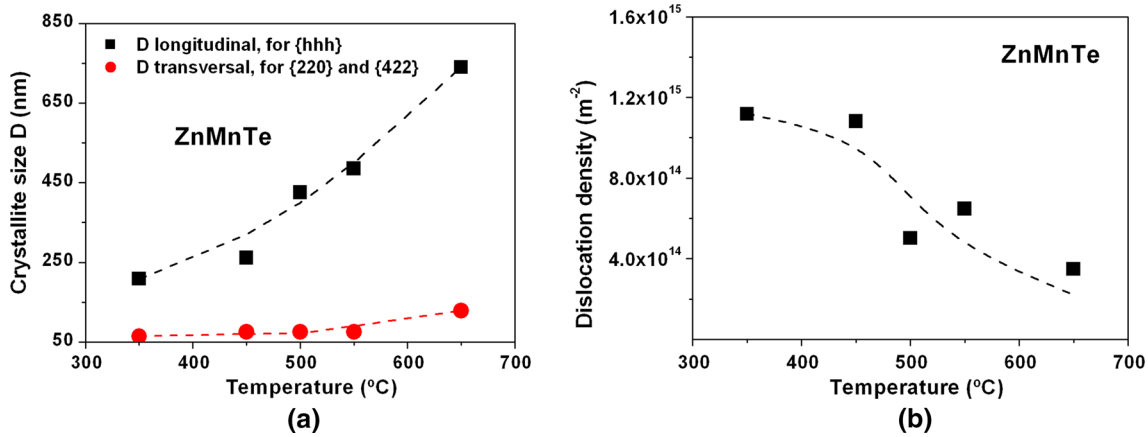

Fig. 8—(*a*) Crystallite size and (*b*) dislocations density from ZnMnTe films deposited over glass at various substrate temperatures [from 623 K to 923 K (350 °C to 650 °C)]. The dashed lines are a guide for the eye.

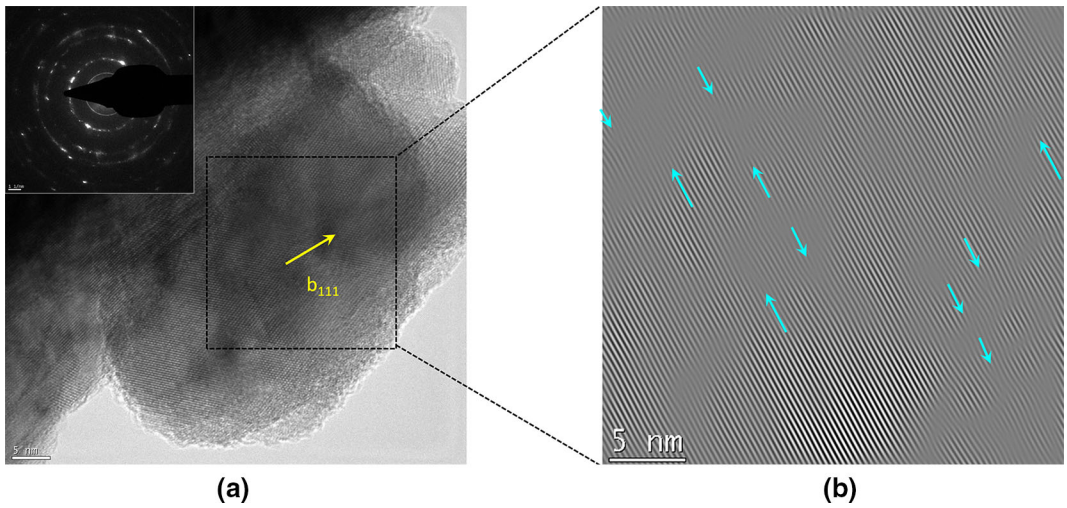

Fig. 9—(*a*) HRTEM image of a ZnMnTe film grown on glass at a substrate temperature of 623 K (350 °C). The arrow indicates the direction of the Burger's vector for the screw dislocations, the same as the axis of this type of dislocation. (*b*) Inverse FFT (IFFT) filtered image of crystallite showing the distribution of dislocations along the [111] direction. The arrows mark some of the screw dislocations that can be observed in the squared area of the FFT image.

dislocation distribution.[6] Calculated values as a function of the substrate temperature are shown in Figure 8(b).

The average dislocation density is slightly temperature dependent, maintaining a value of about 1×10^{15} m^{-2} at low and mean temperatures and reducing its value until about 2×10^{14} m^{-2} when the growth is made at the higher temperature of 923 K (650 °C).

The presence of dislocations is confirmed by HRTEM. Figure 9(a) shows the HRTEM image of a crystallite of a ZnMnTe film grown at 623 K (350 °C) in which the direction of the Burger's vector has been indicated. For screw (111) dislocations, the Burger's vector, the dislocation line, and the axis of the screw dislocation follow the same direction. In Figure 9(b), the Inverse FFT (IFFT) filtered image of this previous image is shown which reveals the distribution of dislocations along the [111] direction. The arrows in Figure 9(b) mark some of the screw dislocations that can be observed in the squared area of the FFT image. Similar images for the lower temperature samples exhibit a higher concentration of dislocations, thus confirming the results obtained by XRD.

IV. ANALYSIS AND DISCUSSION

Doping process can induce structural changes in the parent material. One of the most important aspects is if the added atoms are incorporated into the crystal structure of the host or if they induce the formation of additional phases. Additionally, the dopant can affect the substructural characteristics of the host by influencing the shape or size of crystallites. In our case, we have studied the structural and substructural characteristics of Mn-doped ZnTe. As shown, several experimental and theoretical techniques must be applied in a combined form to have significant insights about the morphological, structural, and substructural characteristics of

films. This methodology of work allow of obtaining information from different methods and a comparison between calculated and experimental values. As a special issue, we have made use of the intrinsic anisotropy of the XRD peak broadening to obtain the average shape and size of crystallites.

Related with the structural characteristics, powder diffraction reveals that films have a cubic structure with a (111) preferred orientation, independently of the dopant quantity observed in the temperature range here considered. Analysis of the lattice constant shows an enlargement with the Mn content, thus indicating that Mn atoms have penetrated into the ZnTe lattice. By analyzing the characteristics of the Mn^{2+} ions, the enlargement of the lattice constant suggests that the Zn^{2+} ions are partially substituted by the Mn^{2+} ions with a high spin state. Mn concentration has been determined from calculated values through the Vegard's law and from EDS measurements. Obtained values have shown that the quantity of Mn is lower than the nominal value and that this quantity is decreased as the substrate temperature is increased. This behavior is explained after analyzing the size of crystallites as a function of the substrate temperature. As crystallites result to be bigger with temperature, the surface to volume ratio is decreased, consequently becoming more difficult the penetration of Mn^{2+} ions.

Morphological analysis by SEM shows that the films are composed by columnar grains with widths that enlarge as the substrate temperature increases, but decreasing its density and maintaining the thickness of the layer. This indicates that the width of grains depends on the substrate temperature but the deposited quantity of material is temperature independent.

In order to have more detailed information about the shape and size of crystallites, the broadening of the XRD peaks must be analyzed. It has been found a strong diffracting anisotropy of films revealed by the classical Williamson–Hall method. This has lead to apply the modified Williamson–Hall plot finding that, in addition, the size of crystallites was also dependent on the order of diffraction. This method allows determine the shape and size of crystallites, joined to the density of dislocations associated to the strain enlargement of XRD peaks. It has been found that crystallites are elongated in the direction of growth with the (111) direction as the prismatic axis. This characteristic is a consequence of the columnar growth and, in turns, it is responsible of the marked out-plane preferred orientation of films. Columnar growth is usually explained by a faster growth in a particular direction. On noncrystalline substrates, generally nuclei grow in a random orientation, but if the growth is faster in a privileged direction, this orientation eventually outgrows the other orientations and becomes dominant. On the contrary, in-plane orientation has resulted to be random in the azimuthal angle, providing a uniaxial orientation or fiber texture to grown films. The calculated size of crystallites (length and width) is lower than that observed by SEM, thus indicating that grains are polycrystalline in nature. As before said, these values result to increase with the substrate temperature, becoming crystallites longer and wider as the temperature goes up. Otherwise, the density of dislocations decreases as the substrate temperature increases. The increasing size and the lowering of defects are both indicative of a better crystalline quality of films. In our case, this behavior leads to a reduced penetration of Mn ions, being thus indicative of one of the difficulties in dopping with Mn the parent ZnTe.

V. CONCLUSIONS

A combined methodology of SEM, HRTEM, XRD, and HRXRD measurements has been worked on to determine structural and substructural properties of films. In order to know its applicability, it has been tested on ZnMnTe films grown on glass by the CSVS technique. The behavior of these characteristics has been studied as a function of substrate temperature.

SEM measurements have shown that the growth of films is in the form of columnar polycrystalline grains. XRD measurements have given the orientation and mean size of these elongated grains. The longer dimension is perpendicular to the (111) planes and grains grow in vertical position, providing to films a (111) preferred out-plane orientation. Crystallite size increases with substrate temperature in an anisotropic form. Grains grow faster in the vertical direction rather in the transversal one, thus increasing also their aspect ratio (length/width) with the temperature. From HRXRD pole figures, it is determined that, although there is not in-plane preferred orientation, the most of the columnar grains (90 pct) present the same (111) preferred orientation within an inclination of ± 10 deg.

The Mn content has been determined from XRD measurements of the lattice parameter and confirmed by EDS. It has been found that Mn incorporation produces an enlargement of the lattice. This indicates that Zn^{2+} ions are partially substituted by the ions of Mn^{2+} which have a high spin state. The decreasing of the Mn content as the substrate temperature increases is interpreted in terms of crystallite size, as bigger crystallites difficult the Mn incorporation.

Williamson Hall plots allow the determination of dislocation density, showing that screw dislocations are the dominant type of defects. Its density decreases as the substrate temperature increases, being about 1×10^{15} m^{-2} at low temperature and 2×10^{14} m^{-2} at high temperature.

This study has shown that a combined methodology (SEM, HRTEM, XRD, and HRXRD) gives a complete and ascertained knowledge of the structural and substructural properties of films.

ACKNOWLEDGMENTS

The authors are grateful to the Central Support Service in Experimental Research (SCSIE), University of Valencia, Spain for providing SEM, XRD, HRXRD,

and HRTEM facility. The authors acknowledge funding received from the Spanish Generalitat Valenciana (Projects Nos. ISIC/2012/008 and PrometeoII/2015-004) and Spanish MINECO (Project No. TEC2014-53727-C2-1-R). This work was also supported by the Ministry of Education and Science of Ukraine (Project No. 0116U006813).

REFERENCES

1. J.P. Hirth and J. Lothe: *Theory of dislocations*, McGraw-Hill, New York, 1968.
2. A.J.C. Wilson: *Il Nuovo Cimento*, 1955, vol. 1, pp. 277–83.
3. B.E. Warren and B.L. Averbach: *J. Appl. Phys*., 1950, vol. 21, pp. 595–99.
4. G.K. Williamson and W.H. Hall: *Acta Metall*., 1953, vol. 1, pp. 22–31.
5. T. Ungar and A. Borbely: *Appl. Phys. Lett*., 1996, vol. 69, pp. 3173–75.
6. A. Révész, T. Ungár, A. Borbely, and T. Lendvai: *J. Nanostruc. Mater*., 1988, vol. 7, pp. 779–88.
7. T. Story: *Acta Phys. Pol. A*, 1998, vol. 94, pp. 189–97.
8. D. Ferrand, J. Cibert, A. Wasiela, C. Bourgognon, S. Tatarenko, G. Fishman, T. Andrearczyk, J. Jaroszyński, S. Koleśnik, T. Dietl, B. Barbara, and D. Dufeu: *Phys. Rev. B*, 2001, vol. 63, p. 085201.
9. H.J. Masterson and J.G. Lunney: *Appl. Surf. Sci*., 1995, vol. 86, pp. 154–59.
10. G. Romera-Guereca, J. Lichtenberg, A. Hierlemann, D. Poulikakos, and B. Kang: *Exp. Therm. Fluid Sci*., 2006, vol. 30, pp. 829–36.
11. D. Zeng, W. Jie, H. Zhou, and Y. Yang: *Nucl. Instrum. Methods A*, 2010, vol. 614, pp. 68–71.
12. A. Zozime, M. Seibt, J. Ertel, A. Tromson-Carli, R. Druilhe, C. Grattepain, and R. Triboulet: *J. Cryst. Growth*, 2003, vol. 249, pp. 15–22.
13. J. Huang, L.J. Wang, K. Tang, and R. Xu: *Phys. Procedia*, 2012, vol. 32, pp. 161–64.
14. G. Kostorz, H.A. Calderon, and J.L. Martin: *Fundamental aspects of dislocation interactions: low-energy dislocation structures III (eBook)*, Kobo Edition, Elsevier, Lausanne, 2013.
15. D. Kurbatov, A. Opanasyuk, S.M. Duvanov, A.G. Balogh, and H. Khlyap: *Solid State Sci*., 2011, vol. 13, pp. 1068–71.
16. V. Kosyak, A. Opanasyuk, P.M. Bukivskij, and Y.P. Gnatenko: *J. Cryst. Growth*, 2010, vol. 312, pp. 1726–30.
17. P.F. Fewster: *Rep. Prog. Phys*., 1996, vol. 59, pp. 1339–1407.
18. M. Imamura and T. Yamaguchi: *J. Phys. Conf. Ser*., 2010, vol. 200, p. 062009.
19. R.D. Shannon: *Acta Cryst. A*, 1976, vol. 32, pp. 751–67.
20. A. Avdonin, L. Van Khoi, W. Pacuski, V. Domukhovski, and R.R. Galazka: *Acta Phys. Pol. A*, 2007, vol. 112, pp. 407–14.
21. E. Dynowska and E. Przezdziecka: *J. Alloys Compd*., 2005, vol. 401, pp. 265–71.
22. E. Janik, E. Dynowska, J. Bak-Misiuk, M. Leszczyński, W Szuszkiewicz, T Wojtowicz, G Karczewski, and AK Zakrzewski: *J. Kossut Thin Solid Films*, 1995, vol. 267, pp. 74–78.
23. P. Djemia, Y. Roussign, and A. Stashkevich: *Acta Phys. Pol*., 2004, vol. 106, pp. 239–47.
24. G.B. Harris: *Philos. Mag*., 1952, vol. 43, pp. 113–23.
25. W. Mahmood and N.A. Shah: *Curr. Appl. Phys*., 2014, vol. 14, pp. 282–86.
26. C.V. Thompson and R. Carel: *Mater. Sci. Eng. B*, 1995, vol. 32, pp. 211–19.
27. E. Mittemeijer and Z.U. Welzel: *Kristallogr*, 2006, vol. 223, pp. 552–60.
28. M.A. Krivoglaz: *Theory of X-ray and thermal neutron scattering by real crystals*, Plenum Press, New York, 1969.
29. T. Ungár, S. Ott, P.G. Sanders, A. Borbely, and J.R. Weertman: *Acta Mater*., 1998, vol. 46, pp. 3693–99.
30. T. Ungár: *Mater. Sci. Forum*, 1998, vols. 278–281, pp. 151–57.
31. T. Ungar, I. Dragomir-Cernatescu, D.L. Louer, and N. Audebrand: *J. Phys. Chem. Solids*, 2001, vol. 62, pp. 1935–41.
32. Y. Wang, S.L.I. Chan, R. Amal, Y.R. Shen, and K. Kiatkittipong: *Adv. X-ray Anal*., 2010, vol. 54, pp. 92–100.
33. B.H. Lee: *J. Appl. Phys*., 1970, vol. 41, pp. 2984–90.
34. Y. Nishi and R. Doering: *Handbook of Semiconductor Manufacturing Technology*, 2nd ed., CRC Press, Boca Raton, 2007.
35. T. Ungar, I. Dragomir, A. Revesz, and A. Borbely: *J. Appl. Cryst*., 1999, vol. 32, pp. 992–1002.
36. M.P.C. Kalita, K. Deka, J. Das, N. Hazarika, P. Dey, R. Das, S. Paul, T. Sarmah, and B.K. Sarma: *Mater. Lett*., 2012, vol. 87, pp. 84–86.